Manuscript 8008 - Revision 1:

Gold speciation in hydrothermal fluids revealed by in situ high energy resolution X-ray absorption spectroscopy

Gleb S. Pokrovski[1*], Elsa Desmaele[2], Clément Laskar[1], Elena F. Bazarkina[3,4], Denis Testemale[3], Jean-Louis Hazemann[3], Rodolphe Vuilleumier[2], Ari Paavo Seitsonen[2], Guillaume Ferlat[5], Antonio Marco Saitta[5]

[1]Experimental Geosciences Group (GeoExp), Géosciences Environnement Toulouse (GET), UMR 5563, Observatoire Midi-Pyrénées, Université de Toulouse, Centre National de la Recherche Scientifique (CNRS), Institut de Recherche pour le Développement (IRD), 14, avenue Edouard Belin, F-31400 Toulouse, France

[2]PASTEUR, Département de Chimie, École Normale Supérieure, PSL University, Sorbonne Université, CNRS, F-75005 Paris, France

[3]Université Grenoble Alpes, CNRS, Institut Néel, 25, avenue des Martyrs, F-38042 Grenoble Cedex 9, France

[4]Institute of Geology of Ore Deposits, Petrography, Mineralogy and Geochemistry, Russian Academy of Sciences (IGEM RAS), 35, Staromonetny per., F-119017 Moscow, Russia

[5]Sorbonne Université, CNRS, UMR 7590, IMPMC, F-75005 Paris, France

* Corresponding author: phone: (33)-(0)5-61-33-26-18; fax: (33)-(0)5-61-33-25-60;
e-mail: gleb.pokrovski@get.omp.eu; glebounet@gmail.com

Revision 1 for American Mineralogist

17 May 2021

Paper Highlight Information
Please write a description of your paper and its implications at a level that a broad geoscience/materials science audience would comprehend. Please keep your description to 500 characters or less. A graphic illustrating the key findings is highly desirable in addition to or in place of the words. To add a figure, go back to File upload and add a Graphical Abstract. This will be used on our web page (http://www.minsocam.org/MSA/Ammin/AM_NotableArticles2019.html), MSA-talk, and potentially other venues to help readers and researchers find your paper.

A combination of in situ spectroscopy and molecular modeling reveals the identity, structure, and stability of the major aqueous complexes transporting gold by hydrothermal fluids and highlights an important role of the trisulfur ion in gold transfer and concentration in hydrothermal-magmatic deposits of subduction zones. Our approach opens perspectives for studies of metals in geological fluids, and potentially silicate melts, inaccessible to direct observation in nature.

ABSTRACT

Gold mobilization, transfer and concentration in the Earth's crust are controlled by hydrothermal sulfur- and chloride-bearing fluids. Yet the exact chemical identity, structure and stability of Au-bearing species and, in particular, the respective contributions of the sulfide (HS^-) and trisulfur ion ($S_3^{\bullet-}$) ligands to Au transport lack direct in situ evidence. Here we employed high energy resolution fluorescence detection - X-ray absorption spectroscopy (HERFD-XAS) on aqueous sulfate/sulfide/$S_3^{\bullet-}$-bearing solutions at typical hydrothermal temperatures and pressures (T = 350°C, P = 600 bar) to reveal differences in dissolved Au spectral signatures indicative of contrasting fluid-phase Au speciation as a function of acidity and redox conditions. Combined with in situ Au solubility measurements and quantum-chemical and thermodynamic modeling, our spectroscopic data provide direct evidence for the $Au(HS)S_3^-$ and $Au(HS)_2^-$ complexes predominant at acidic-to-neutral and alkaline conditions, respectively. Our findings thus directly confirm a recent speciation scheme for Au in aqueous S-bearing fluids established using less direct methods, and highlight an important role of the trisulfur ion in gold mobilization and concentration in hydrothermal-magmatic deposits associated with subduction zones. More generally, our results show that HERFD-XAS enables the identification of structural and coordination features in metal complexes virtually unresolvable using classical XAS techniques. By avoiding limitations of less direct techniques, our integrated high-resolution spectroscopic approach opens perspectives for studies of the speciation and solubility of gold and other metals in high T-P fluids, and potentially silicate melts, inaccessible to direct observation in nature.

Keywords: gold, sulfur, trisulfur radical ion, hydrothermal fluid, ore deposit, high energy resolution fluorescence detection - X-ray absorption spectroscopy (HERFD-XAS), X-ray absorption near edge structure (XANES), solubility, density functional theory (DFT), first principles molecular dynamics (FPMD).

INTRODUCTION

Gold deposits on Earth result from an exceptional concentration phenomenon yielding metal contents in ore a thousand to a million times higher than those in most crustal and mantle rocks whose Au average abundance is of ~1 ppb (Frimmel 2008; Saunders et al. 2018). This spectacular enrichment process is ensured by aqueous fluids transporting gold mostly as sulfide- and chloride-types of complexes (e.g., Helgeson and Garrels 1968; Boyle 1969; Seward 1989; Garofalo et al. 2014). However, the exact chemical identity and stability of such complexes and their capacity to carry the noblest metal of the Periodic Table yet remain controversial. Most available studies, conducted using traditional solubility methods applied to hydrothermal-magmatic fluids (e.g., see Pokrovski et al. 2014 for an overview), generally agree that the most likely Au-bearing species are the aurous (Au^I) dichloride ($AuCl_2^-$) common in acidic, saline, oxidized conditions, and the dihydrogen sulfide ($Au(HS)_2^-$) dominant in neutral to basic, S-bearing, reduced fluid compositions. In contrast, the role of other potentially important Au^I-bearing ligands such as polysulfide radical ions ($S_2^{\bullet-}$ and $S_3^{\bullet-}$) has not been yet definitely recognized, despite the growing body of studies demonstrating that these sulfur forms are stable across a wide temperature (*T*) and pressure (*P*) range of acidic-to-neutral sulfate/sulfide-bearing hydrothermal-magmatic fluids associated with subduction zones (Pokrovski and Dubrovinsky 2011; Jacquemet et al. 2014; Pokrovski and Dubessy 2015; Barré et al. 2017; Schmidt and Seward 2017; Colin et al. 2020). The lack of direct data on gold-sulfur radical ion interactions is mostly because the gold solubility pattern is a complex function of various fluid parameters such as acidity, chlorinity, redox, and S speciation. This complexity makes it difficult a straightforward and unambiguous analysis of bulk solubility data in terms of aqueous species identity, in particular in the absence of more direct in situ molecular-level information (e.g., Pokrovski et al. 2014, 2019).

Synchrotron-based X-ray absorption spectroscopy (XAS) is the most direct in situ method for providing such information about the first-shell coordination environment and the identity and number of ligands around the metal in an aqueous complex. In the last 20 years, this method has emerged as a key complement to the traditional solubility approach in hydrothermal fluids for a number of metals and metalloids (e.g., Pokrovski et al. 2002, 2005; Bazarkina et al. 2014; Brugger et al. 2016; Testemale et al. 2004, 2011; references therein), including gold (e.g., Pokrovski et al. 2009a,b, 2015; Trigub et al. 2017a; Tagirov et al. 2019). However, the traditional XAS method is weakly sensitive to light elements (e.g., H in HS^{-}-type ligands) and beyond-the-nearest-shell atoms (e.g., polysulfide ligands Au-S-(S_n) or alkali ion pairs Au-Cl-Na/K), as well as to ligands with similar atomic numbers (e.g., S-16 vs Cl-17). As a result, questions yet remain open about the identity and abundance of Au aqueous complexes with polysulfide ions in S-bearing hydrothermal fluids (e.g., Pokrovski et al. 2009a, 2015; Mei et al. 2013; Trigub et al. 2017a), as well as about the significance of alkali-ion pairs of the anionic chloride and sulfide Au species in magmatic fluids (e.g., $NaAuCl_2^0$, $KAu(HS)_2^0$; Zajacz et al. 2010, Mei et al. 2014; Tagirov et al. 2019). These limitations of traditional XAS are particularly severe in the case of aurous species, which all have quasi-linear first-shell geometries L-Au^I-L and very similar Au^I-L interatomic distances (where L is the Cl or S ligand; Pokrovski et al. 2009a,b).

Recent developments in high energy resolution fluorescence detection - X-ray absorption spectroscopy (HERFD-XAS) devices on synchrotron beamlines potentially enable to overcome these fundamental limitations of traditional XAS, making it possible to i) reveal spectral features poorly resolved using standard XAS detection techniques employing solid-state detectors, and ii) significantly increase signal-to-noise ratio especially for dilute systems such as metals in fluids or trace elements in complex mineral matrixes (e.g., Proux et al. 2017). Whereas HERFD-XAS methods are increasingly applied to study redox and structural state of trace elements such as gold in major sulfide minerals and catalytic materials (e.g., van Bokhoven et al. 2006; Trigub et al. 2017b, Merkulova et al. 2019; Pokrovski et al. 2019, 2021), their application to high *T-P* fluids yet remains challenging. In an attempt to provide a more resolved picture of gold-sulfur complexes and to further develop in situ approaches for metals in hydrothermal fluids, here we used HERFD-XAS to directly measure the molecular speciation and solubility of gold at 350°C and 600 bar in two model aqueous S-bearing fluids representative of those that have formed hydrothermal gold deposits. Combined with atomistic simulations of Au complexes and thermodynamic calculations of sulfur and gold speciation, our results provide direct evidence for gold-trisulfur ion complexes in hydrothermal fluids and open further perspectives for studying, using HERFD-XAS approaches, the metal speciation and transport by fluids and melts in the lithosphere.

METHODS

Experimental strategy and conditions

Gold solubility and Au L_3-edge HERFD-XAS spectra in the aqueous phase have been measured at 350°C and 600 bar for two fluid compositions of contrasting pH and redox parameters (Table 1, Fig. 1a,b) at which two different Au-S complexes were predicted to be dominant according to the available thermodynamic data (Pokrovski et al. 2014, 2015), $Au(HS)S_3^-$ (experiment 1) and $Au(HS)_2^-$ (experiment 2), formed according to the formal dissolution reactions:

$$Au(s) + H_2S + S_3^{\bullet-} + \frac{1}{4} O_2 = Au(HS)S_3^- + \frac{1}{2} H_2O \quad (1)$$

$$Au(s) + H_2S + HS^- + \frac{1}{4} O_2 = Au(HS)_2^- + \frac{1}{2} H_2O \quad (2)$$

Our choice of fluid compositions is based on extensive literature data of Au solubility and traditional XAS measurements in thiosulfate solutions. Thiosulfate is non-toxic and stable at ambient temperature making it easy to handle and accurately load into the optical cell; it breaks down to sulfate, sulfide and $S_3^{\bullet-}$ on heating, providing the source of sulfur ligands (e.g., Jacquemet et al. 2014; Pokrovski et al. 2015; Kokh et al. 2020):

$$S_2O_3^{2-} + H_2O = SO_4^{2-} + H_2S \quad (3)$$

$$19\ H_2S + 5\ SO_4^{2-} + 2\ H^+ = 8\ S_3^{\bullet-} + 20\ H_2O \quad (4)$$

The addition of acid (HCl) or base (KOH or NaOH) to the initial thiosulfate solution enables controlled pH value choice and buffering:

$$SO_4^{2-} + H^+ = HSO_4^- \quad (5)$$

$$H_2S = HS^- + H^+ \quad (6)$$

Equilibrium between the dominant sulfate and sulfide species at elevated temperatures (>250°C) imposes oxygen fugacity (f_{O_2}) ranging from ~HM+1 at acidic pH to ~HM–1.5 at neutral-to-basic pH (where HM denotes the log f_{O_2} value of the conventional hematite-magnetite mineral buffer):

$$H_2S + 2\ O_2 = SO_4^{2-} + 2\ H^+ \quad (7)$$

In addition, ion pairs of the sulfate and sulfide anions with alkalis (K^+) along with minor amounts of SO_2, molecular sulfur (S_8, both aqueous and molten), and polysulfide dianions S_n^{2-} contribute to aqueous sulfur speciation, depending on pH, as predicted using the available thermodynamic data and shown in Fig. 1a (see Kokh et al. 2020 for details and data selection). It can be seen that the two experimental compositions chosen here significantly differ in terms of pH, redox, and HS^- and $S_3^{\bullet-}$ ligand concentration, leading to an Au speciation contrast according to reactions (1) and (2). Not only our chosen compositions and *T-P* conditions provide robust constraints on the experimental system, but they do also offer a good analog for natural S-rich (to several wt% S) fluids in arc-related magmatic-hydrothermal porphyry Cu-Au-Mo and associated epithermal deposits at *T* of 200–500°C, *P* of 100–1000 bar, a wide pH (3–8) and redox (HM±2) range, where sulfate and sulfide coexist (Einaudi et al. 2003; Kouzmanov and Pokrovski 2012).

In situ high-resolution XAS measurements

High energy resolution fluorescence detection - X-ray absorption spectroscopy (HERFD-XAS, hereafter HR-XAS for simplicity) analyses at the Au L_3 edge (11.919 keV) of the two experimental fluids were performed at FAME-UHD (BM16) beamline (Proux et al. 2017) of the European Synchrotron Radiation Facility, Grenoble, France, using a recently developed crystal analyzer spectrometer operating in HERFD mode (Llorens et al. 2012). Compared to conventional XAS spectroscopy, HR-XAS has two major advantages: i) a significant gain in spectral resolution compared to nominal resolution defined by the core hole width of the absorption edge; this gain allows accurate detection of different features in the X-ray absorption near-edge structure (XANES) spectral region, which are indicative of Au coordination environment, but are generally poorly expressed in nominal-resolution spectra (e.g., Pokrovski et al. 2015, 2021), and ii) the ability to efficiently filter out all unwanted contributions from elastic scattering and fluorescence from other elements in the fluid matrix, and thus significantly improve both the limit of detection for Au and signal-to-noise spectral ratio. The beamline X-ray optics incorporated a Si(220) doublecrystal monochromator with sagittal focusing (beam spot full width at half maximum at the sample ~100×200 μm^2), Rh-coated mirrors for harmonic rejection, and a crystal analyzer spectrometer with 3 Si(660) crystals under He(gas) atmosphere in a Rowland circle geometry (1-meter diameter). The experimental spectral resolution was measured to be 0.9±0.1 eV at the Lα_1 Au fluorescence line, which corresponds to a significant gain in resolution compared to classical mode (core-hole lifetime broadening is 5.54 eV at Au L$_3$-edge; Campbell and Papp, 2001). High-resolution fluorescence XANES, together with EXAFS (extended X-ray absorption fine structure), spectra were recorded using a Vortex EX-90 mono-element detector. The use of such an energy-resolved detector (bandwidth ~200 eV) allowed counting the photons diffracted by the spectrometer crystals in Bragg conditions for Au Lα_1 (Bragg's angle = 85.71°) and removal of all other contributions due to energy-resolved detection, thereby greatly improving the resulting signal-to-noise ratio. Transmission (nominal-resolution) spectra were simultaneously recorded using silicon diodes collecting scattered radiation from a Kapton foil placed in the incident and transmitted X-ray beam. Energy calibration of each scan was checked using a gold metal foil whose L$_3$-edge energy was set to 11,919.0 eV as the maximum of the spectrum first derivative. The accuracy of this calibration over the whole experimental duration is about ±0.5 eV.

Experiments were carried out using a hydrothermal autoclave developed at the Néel Institute (Testemale et al. 2005) and described in detail elsewhere (Pokrovski et al. 2006). The runs were conducted at 350±2 °C and 600±1 bar by allowing a piece of gold foil to react with an aqueous thiosulfate solution in the glassy-carbon inner cell, and following the established procedures (Pokrovski et al. 2009a,b). To enable the HR-XAS measurements, the autoclave was tilted from its vertical position to match the required Bragg angle of the crystal analyzers (Fig. 2). Multiple XAS scans were recorded as a function of time both to monitor the eventual spectra evolution and to improve spectral statistics. No changes in the spectra, which might arise from X-ray beam-induced photochemical phenomena or reactions with the cell walls, were detected (apart from minor evolution of total Au dissolved concentrations, see Supplemental Materials). The absence of such phenomena is in agreement with both the stability of Au-S species in well-buffered systems as those of this and previous (e.g., Pokrovski et al. 2009a) studies, and the known chemical inertness of the glassy-carbon cell material (Pokrovski et al. 2006). Dissolved Au concentrations in the fluid were estimated using two independent methods i) from the amplitude of the absorption edge height of the Au L$_3$-edge transmission spectra from the classical X-ray absorption relation and using the known fluid density and absorption path length through the cell (e.g., Pokrovski et al. 2005, 2009a), and ii) from the amplitude of the fluorescence spectrum corrected for X-ray absorption by the fluid and calibrated using a $HAuCl_4$ standard solution of known Au concentration (see Table S1, Fig. S1, and Supplementary Text).

In this study, we focus on the HR-XANES spectral region because the extended X-ray absorption fine structure (EXAFS) region is not significantly affected by the energy-resolution improvement and has been the subject of extensive detailed work (Pokrovski et al. 2009a, 2015) that could not reveal any significant differences in the EXAFS signal for different Au^I-(poly)sulfide type of complexes in the fluid.

Quantum-chemistry ab-initio modeling of XANES spectra using FDMNES

Direct and unambiguous interpretation of XANES spectra, particularly in high-resolution mode, would ideally require reference compounds with Au molecular environments being as close as possible to those of the samples. Because of the lack of such reference compounds for aqueous Au-HS-S_n type complexes, a theoretical simulation of XANES spectra is the method of choice. The rapidly growing application of this method to synthetic and natural materials has been boosted by recent progress in quantum-chemical modeling of full electron potential in the near-edge absorption region, coupled with increasing computer power enabling the use of Finite Difference (FD) methods for solving the Schrödinger equation on the node points of a three-dimensional grid (Amestoy et al. 2006; Guda et al. 2015) as implemented in the FDMNES code (Joly 2001, 2020; Bunau and Joly 2009). Using this code, we simulated Au L_3-edge HR-XANES spectra of most plausible Au^I complexes with H_2O, HS^- and $S_3^{\bullet -}$ ligands whose optimized geometries were generated using Density Functional Theory (DFT) calculations, including both geometry optimizations (static DFT) and First Principles Molecular Dynamics (FPMD) simulations (see next section). The generated XANES spectra were then compared with the experimental ones. Calculations were performed in FD mode and accounting for relativistic effects and spin-orbit interactions intrinsic to heavy atoms such as gold and using self-consistent potentials allowing accurate determination of the Fermi energy level (code keywords *SCF, Relativism, Spinorbit*). The obtained raw calculations are further convoluted with a Lorentzian function (keyword *Arc*) with a width of 0.9 eV (keyword *Gamma_hole*) corresponding to the energy resolution of our HERFD setup. The cluster size (keyword *Radius*) for a given complex was set to the largest Au-atom (S or H) distance in the complex plus 1.2 Å to account for the complete electronic sphere. To account for the presence of a dense medium (solvent) around the Au molecular cluster, the keyword *Vmax* was used (*Vmax* = –6). To allow comparisons in energy position between theoretical and experimental spectra, the simulated convoluted spectra were shifted according to differences in their calculated initial orbital energy (*Epsii*; Joly 2020). This correction has a typical uncertainty of ±0.5 eV, which is comparable to that of the experimental energy calibration. The FDMNES simulations explored the most representative Au-(poly)sulfide species invoked in recent studies based on static DFT and FPMD methods (Mei et al. 2013; Pokrovski et al. 2015; Trigub et al. 2017a).

DFT and FPMD data for optimized complex geometries

Static DFT calculations of relaxed geometries for five key Au aqueous complexes, $Au(HS)(H_2O)^0$, $Au(HS)S_3^-$, $Au(HS)_2^-$, $Au(S_3)_2^-$ and $AuCl_4^-$, were performed following previously established methods and protocols (Pokrovski et al. 2009a,b, 2015) and using 4 different exchange-correlation functionals, BLYP, B3LYP, PBE, and PBE0 (Becke 1988, 1993; Lee et al. 1988; Perdew et al. 1996a,b). All four functionals yielded Au-S and Au-Cl distances (Supplementary Table S2) to be within <0.05 Å of the EXAFS-derived values from recent experiments (~2.29 Å for Au^I-S and ~2.28 Å for Au^{III}-Cl; Pokrovski et al. 2009a,b, 2015). Each resulting geometry of the Au complexes was used to calculate a XANES spectrum. For a given species, the XANES spectra were found to be almost identical, regardless of the exchange-correlation functional used to generate their geometries. For illustrations in this study, we have therefore chosen those generated using B3LYP, for consistency with the FPMD simulations that used the BLYP functional.

FPMD-generated complex conformations, also used in XANES calculations, were taken from extensive simulations analogous to our previous study of Au^I complexes in hydrothermal solutions (Pokrovski et al. 2015). However, calculating a XANES spectrum from each FPMD snapshot using the FD method would be computationally too demanding in light of the too large number of FPMD snapshots (at least 100) needed to fully represent the FPMD trajectories. Therefore, a limited number of representative conformations from the FPMD simulations for a given Au complex has been extracted using a clustering method (6 configurations per species; see Supplementary Text for details). For each of the 4 selected Au species, the 6 extracted configurations (Supplementary Fig. S2) were used to calculate 6 XANES spectra by the FD method. The resulting spectra, weighted by the cluster size (i.e. number of configurations in each cluster), were then summed up to obtain the average XANES spectrum expected to be representative of the whole set of FPMD snapshots for a given species. Water molecules beyond the first Au atomic shell were also considered in the calculation of the XANES spectra, but were found to have a negligible effect, in agreement with the generally low sensitivity of the XAS signal to distant and distorted shells. The average FPMD-derived Au-S and Au-O distances for the S-bearing Au species are generally ~0.05 Å longer than their DFT-derived counterparts (Supplementary Table S2), but this difference has a minor effect on the calculated XANES spectra. The observed differences in calculated distances using the same BLYP functional and the same basis set are attributed to the use of a pseudopotential for Au^I in FPMD that approximates the effect of core electrons. This approximation is required in FPMD simulations of liquids to significantly reduce the computer time, whereas the far less computationally demanding static DFT methods treat both core and valence electrons explicitly. Similar minor discrepancies in the calculated distances between static DFT and FPMD have also been found for other metals (e.g., Spezia et al. 2008, 2012). The FPMD-derived spectra for the four Au-S species were compared with their static DFT-derived spectra and with the experiment (Supplementary Figs S3 and S4).

RESULTS

Gold solubility

The obtained Au concentrations averaged over all datapoints from transmission and fluorescence scans are 0.004±0.002*m* and 0.007±0.004*m* (±2 standard deviations, s.d.) in experiment 1 and 2, respectively (see Supplemental Material for details). These values are in excellent agreement with equilibrium Au solubility predictions using the thermodynamic properties of sulfur species and Au complexes established in recent studies (Pokrovski et al. 2015; Kokh et al. 2020 and references therein). It can be seen in Fig. 1b that the $Au(HS)S_3^-$ is predicted to be by far the dominant Au species in the acidic run (experiment 1) whereas the concentrations of the traditional sulfide species such as $Au(HS)_2^-$ and $Au(HS)(H_2O)^0$, are 50 to 100 times smaller.

Likewise, in the basic pH run (experiment 2), $Au(HS)_2^-$ is ~100 time more abundant than $Au(HS)S_3^-$. Thus, our measurements provide robust independent support of the recently suggested Au speciation scheme involving the Au-trisulfur ion complex, which plays an important role in acidic-to-neutral S-rich fluids (Pokrovski et al. 2015, 2019), whereas the traditional hydrogen sulfide complex $Au(HS)_2^-$ quantitatively accounts for Au speciation and solubility in neutral to moderately alkaline fluids (e.g., Seward 1973; Pokrovski et al. 2009a, 2014). Our new data, together with recent extensive both in situ and ex situ experiments within the hydrothermal *T-P* range (200-500°C, <1 kbar), do not provide evidence for additional or alternative Au-S-type complexes invoked in some older studies conducted before the discovery of the trisulfur ion (e.g., $Au(HS)(H_2S)^0$, $Au(HS)(SO_2)^0$, $Au(HS)(H_2S)_3^0$, $Au_2(HS)_2S^{2-}$; Seward 1973; Hayachi and Ohmoto 1991; Loucks and Mavrogenes 1999; Pokrovski et al. 2009a), even though it cannot be fully excluded that these or other species might be present in aqueous fluids outside the *T-P*-compositional range covered so far. The contrasting Au speciation evidenced by our solubility experiments and thermodynamic modeling allows us to further evaluate the applicability of the HR-XAS method combined with molecular modeling to distinguish among the different Au-S species.

Gold HR-XANES spectra

It can be seen in Fig. 3 that the use of HERFD mode provides a spectacular improvement in the spectral resolution, with each spectral feature neatly emphasized and before-edge absorption removed, compared to 'traditional' fluorescence or transmission acquisition modes. For example, the HR-XANES spectrum of the $AuCl_4^-$ complex from a standard $HAuCl_4$ solution used for calibration (Fig. 3a) is characterized by a very intense pre-edge feature due to 2p-5d electron transition typical for square-planar coordinated Au^{III} compounds (e.g., Pokrovski et al. 2009b) and at least 3 distinct post-edge resonances, whereas all these features are significantly damped in the nominal-resolution spectrum. Likewise, the HR-XANES spectra of Au^{I} sulfur complexes from both hydrothermal experiments show a neatly expressed narrow white line at ~11,920 eV and an intense post-edge resonance at ~11,930 eV, whereas their transmission spectra exhibit high noise and barely distinguishable weak resonances (Fig. 3b). Note that even though nominal-resolution fluorescence spectra on similar solutions, using longer acquisition times and higher Au concentrations recorded in recent studies, were characterized by higher signal-to-noise ratios (Pokrovski et al. 2009a, 2015), they still had poorly resolved spectral shapes (Fig. 3b).

By contrast, there are small but systematic differences in HR-XANES spectra of the two experiments here, with a higher magnitude of the white line and a larger width of the post-edge resonance with its tail shifted to higher energies for experiment 1, as apparent in Fig. 4. Because the exact electronic-level interpretation of the origin of different XANES spectra resonances for aqueous species of the same metal redox state and coordination is rather difficult at present, here we have chosen a more empirical, but far more practical, approach by direct comparisons with FDMNES-simulated XANES spectra of different Au-S species whose structures were either generated by static DFT calculations or extracted from FPMD configurations as 6 representative geometric clusters averaged according to their respective weights (Supplementary Material and Fig. S3). It can be seen in Fig. 4 that these theoretical XANES spectra of $Au(HS)_2^-$ and $Au(HS)S_3^-$ exhibit essentially the same differences as the experimental spectra, with higher white-line amplitude and a first post-edge main resonance shift towards higher energies for the $Au(HS)S_3^-$ cluster. Note that minor variations in the geometry and Au-ligand interatomic distances of structures generated by both static DFT with different exchange-correlation functionals, and averaged FPMD clusters extracted from a large number of snapshots, were found to produce rather similar FDMNES-calculated XANES spectra for a given species, but distinct energy positions and resonance features among the different species (Supplementary Fig. S3). It is thus concluded that, at least in the case of Au^I-S complexes formed at our conditions, the observed differences in the HR-XANES spectra are mostly due to the presence of additional S-atoms in the next-nearest shell of

Au, arising from the $S_3^{\bullet-}$ ligand. Note that neither EXAFS nor lower-resolution XANES spectra (Pokrovski et al. 2009a, 2015; Trigub et al. 2017a) were able to provide such evidence that can only be gained from HR-XANES data such as those of the present study.

Furthermore, XANES spectra for two other, more stoichiometrically and structurally contrasting, Au^I-S complexes, $Au(HS)(H_2O)^0$ and $Au(S_3)_2^-$, were also modeled using the FDMNES code (Figs 5 and S4). As expected, the spectra of each species strongly contrast in shape and show significant energy shifts and amplitude differences compared with the experimental spectra. These differences further attest to the much smaller (if any) contributions of those species to the Au fluid-phase speciation and the resulting gold solubility measured in this study, as also confirmed by thermodynamic predictions (e.g., Fig. 1). As a conclusion, our data provide direct spectroscopic evidence, which could only be gained using high-resolution XAS methods, for the existence of the $Au(HS)S_3^-$ complex in hydrothermal fluids. Its existence is also consistent with available less direct spectroscopic, solubility, and molecular simulations acquired so far and interpreted by taking account of the $S_3^{\bullet-}$ ion in the aqueous sulfur speciation scheme (Mei et al. 2013; Pokrovski et al. 2015, 2019).

IMPLICATIONS

The key implications of this work are the following.

Our results highlight the potential of the high-resolution XAS methods for in situ studies of metal speciation in aqueous fluids at elevated temperatures and pressures and, in particular, for resolving rather minor atomic-level differences in aqueous species structures and coordination environment, otherwise inaccessible by classical spectroscopy methods (Fig. 4). Behind these small structural differences are ‘hidden’, however, large differences in complex stoichiometry and ligand identity that greatly impact the overall metal solubility and mobility in geological fluids (Fig. 1). As a result, to be fully successful in resolving chemical speciation, high-resolution spectroscopy should be combined with direct metal solubility measurements and thermodynamic and molecular modeling.

Through this combination, our study offers new insight into the long-standing debate about how gold could be massively carried by hydrothermal fluids and form large economic deposits on Earth. In particular, our study provides direct spectroscopic confirmation of the importance of sulfur radical species, such as the trisulfur ion $S_3^{\bullet-}$, for transporting gold in geological fluids. Gold-$S_3^{\bullet-}$ complexes operate within the acidic-to-neutral pH range of sulfide/sulfate-bearing hydrothermal fluids at temperatures above 300°C, by significantly increasing Au solubility and mobility compared to common Au complexes with Cl^- and HS^- ligands traditionally considered in economic geology and geochemistry research. As such, $S_3^{\bullet-}$ may significantly contribute to gold transfer and concentration in the convergent margin geodynamic settings hosting porphyry Cu-Au-Mo and related deposits, which are characterized by large S fluxes and redox conditions of the sulfide-sulfate(-sulfur dioxide) coexistence (e.g., Hedenquist and Lowenstern 1994; Einaudi et al. 2003; Kouzmanov and Pokrovski 2012), which are all favorable for $S_3^{\bullet-}$ (Colin et al. 2020).

Furthermore, the high capacity of $S_3^{\bullet-}$ to solubilize gold in solution may, potentially, be used to improve both the efficiency and safety of methods of gold recovery from ore that yet employ highly toxic chemicals such as cyanide or mercury harmful to the environment (e.g., Adams 2005). The $S_3^{\bullet-}$ ligand may also be exploited in aqueous-media synthesis of gold nanomaterials that uses organic thiol ligands for stabilizing gold nanoparticles in solution and controlling their specific properties (e.g., Häkkinen 2012).

Further developments of integrated HR-XAS methods, which combine both in situ solubility and structural measurements with physical-chemical modeling, applied to magmatic-hydrothermal fluids (and potentially silicate melts) at elevated *T*-*P*, are expected to help in clarifying other yet poorly known aspects of gold speciation and its ubiquitous link with sulfur. Those concern, for example, the effect of traditional polysulfide ligands S_n^{2-}, which may be abundant in low-temperature (<150°C) hydrothermal systems (e.g., Bernd et al. 1994), and of the $S_2^{\bullet-}$ radical ion that is stable at closer-to-magmatic temperatures (>450–500°C; Pokrovski et al. 2019; Colin et al. 2020), as well of mixed-ligand species or alkali-ion pairs (e.g., Na-Cl-HS-S_3; Zajacz et al. 2010), all of them potentially contributing to the exceptional mobility of the most inert metal of the Periodic Table in sulfur-bearing planetary fluids.

ACKNOWLEDGMENTS

This work was funded by the French National Research Agency (grant RadicalS – ANR-16-CE31-0017) and the Institut Carnot ISIFoR (grant OrPet). We acknowledge the European Synchrotron Radiation Facility (ESRF) for access to beam time and infrastructure, and the Grand Equipement National for Calcul Intensif (GENCI) and the Institut du Développement et des Ressources en Informatique Scientifique (IDRIS) for access to high-performance computing facilities. The FAME-UHD project is supported by the French Grand Emprunt EquipEx (EcoX ANR-10-EQPX-27-01), the CEA-CNRS CRG consortium, and the INSU-CNRS. The Cluster of Excellence MATISSE led by Sorbonne University is supported by the ANR Investissement d'Avenir (ANR-11-IDEX-0004-02). I. Kieffer, E. Lahera, O. Proux, and M. Rovezzi are acknowledged for their help with the synchrotron experiments. Special thanks go to Y. Joly for advice on XANES spectra modeling. Comments by Editor D. Neuville and two anonymous referees greatly improved this article.

REFERENCES CITED

Adams, M.D. (2005) *Advances in Gold Ore Processing*. Elsevier.

Amestoy, P.R., Guermouche, A., L'Excellent, J.-Y., and Pralet, S. (2006) Hybrid scheduling for the parallel solution of linear systems. Parallel Computing, 32, 136−156.

Barré, G., Truche, L., Bazarkina, E.F., Michels, R., and Dubessy, J. (2017) First evidence of the trisulfur radical ion S_3^- and other sulfur polymers in natural fluid inclusions. Chemical Geology, 462, 1−14.

Bazarkina, E.F., Pokrovski G.S., and Hazemann J.-L. (2014) Structure, stability and geochemical role of palladium chloride complexes in hydrothermal fluids. Geochimica et Cosmochimica Acta, 146, 107−131.

Becke, A.D. (1988) Density-functional exchange-energy approximation with correct asymptotic behavior. Physical Review A, 38, 3098−3100.

Becke, A.D. (1993) Density-functional thermochemistry. III. The role of exact exchange. Journal of Chemical Physics, 98, 5648−5652.

Berndt, M.E., Buttram, T., Earley, D.III, and Seyfried, W.E. (1994) The stability of gold polysulfide complexes in aqueous sulfide solutions: 100 to 150 °C and 100 bars. Geochimica et Cosmochimica Acta, 58, 587–594.

Boyle, R.W. (1969) Hydrothermal transport and deposition of gold. Economic Geology, 64, 112−115.

Brugger, J., Liu, W., Etschmann, B., Mei, Y., Sherman, D.M., and Testemale, D. (2016) A review of the coordination chemistry of hydrothermal systems, or do coordination changes make ore deposits? Chemical Geology, 447, 219−253.

Bokhoven van, J.A., Louis, C., Miller, J.T., Tromp, M., Safonova, O.V., and Glatzel, P. (2006) Activation of oxygen on gold/alumina catalysts: in situ high-energy-resolution fluorescence and time-resolved X-ray spectroscopy. Angewandte Chemie International Edition, 45, 4651-4654.

Bunau, O., and Joly, Y. (2009) Self-consistent aspects of x-ray absorption calculations. Journal of Physics: Condensed Matter, 21, 345501.

Campbell, J.L., and Papp., T. (2001) Widths of the atomic K-N_7 levels. Atomic Data Nuclear Data Tables, 77, 1–56.

Colin, A., Schmidt, C., Pokrovski, G.S., Wilke, M., Borisova, A.Y., and Toplis, M.J. (2020) *In situ* determination of sulfur speciation and partitioning in aqueous fluid-silicate melt systems. Geochemical Perspectives Letters, 14, 31–35.

Einaudi, M.T., Hedenquist, J.W., and Inan, E.E. (2003) Sulfidation state of fluids in active and extinct hydrothermal systems: transitions from porphyry to epithermal environments (eds. S.F. Simmons and I.J. Graham). Society of Economic Geologists Special Publication, 10, 285–313.

Frimmel, H.E. (2008) Earth's continental crustal gold endowment. Earth and Planetary Science Letters, 267, 45–55.

Garofalo, P.S., Fricker, M.B., Günther, D., Barsani, D., and Lottici, P.P. (2014) Physical-chemical properties and metal budget of Au-transporting hydrothermal fluids in orogenic deposits. Geological Society of London Special Publication, 402, 71–102.

Guda, S.A., Guda, A.A., Soldatov M.A., Lomachenko K.A., Bugaev, A.L., Lamberti, C., Gawelda, W., Bressler, C., Smolentsev, G., Soldatov, A.V., and Joly, Y. (2015) Optimized finite difference method for the full-potential XANES simulations. Application to molecular adsorption geometries in MOFs and metal-ligand intersystem crossing transients. Journal of Chemical Theory Computing, 11, 4512–4521.

Häkkinen, H. (2012) The gold-sulfur interface at the nanoscale. Nature Chemistry, 4, 443–455.

Hayashi, K.I., and Ohmoto, H. (1991) Solubility of gold in NaCl and H_2S-bearing aqueous solutions at 250–350°C. Geochimica et Cosmochimica Acta, 55, 2111–2126.

Helgeson, H.C., and Garrels, R.M. (1968) Hydrothermal transport and deposition of gold. Economic Geology, 63, 622–635.

Hedenquist, J.W., and Lowenstern, J.B. (1994) The role of magmas in the formation of hydrothermal ore deposits. Nature, 370, 519–527.

Jacquemet, N., Guillaume, D., Zwick, A., and Pokrovski, G.S. (2014) In situ Raman spectroscopy identification of the S_3^- ion in S-rich hydrothermal fluids from synthetic fluid inclusions. American Mineralogist, 99, 1109–1118.

Joly, Y. (2001) X-ray absorption near-edge structure calculations beyond the muffin tin approximation. Physical Review B, 63, 125120.

Joly, Y. (2020). FDMNES User's Guide, http://fdmnes.neel.cnrs.fr/.

Kokh, M.A., Assayag, N., Mounic, S., Cartigny, P., Gurenko, A., and Pokrovski, G.S. (2020) Multiple sulfur isotope fractionation in hydrothermal systems in the presence of radical ions and molecular sulfur. Geochimica et Cosmochimica Acta, 285, 100–128.

Kouzmanov, K., and Pokrovski, G.S., 2012. Hydrothermal controls on metal distribution in Cu(-Au-Mo) porphyry systems. Society of Economic Geologists Special Publication 16 (22), 573–618.

Lee, C., Yang, W., and Parr, R.G. (1988) Development of the Colle-Salvetti correlation-energy formula into a functional of the electron density. Physical Reviews, B37, 785-789.

Loucks, R.R., Mavrogenes, J.A. (1999) Gold solubility in supercritical hydrothermal brines measured in synthetic fluid inclusions. Science, 284, 2159–2163.

Llorens, I., Lahera, E., Del Net, W., Proux, O., Braillard, A., Hazemann, J.-L., Prat, A., Testemale, D., Dermigny, Q., Gelebart, F., Morand, M., Shukla, A., Bardou, N., Ulrich, O., Arnaud, S., Berar, J.-F., Boudet, N., Caillot, B., Chaurand, P., Rose, J., Doelsch, E., Martin, P., and Solari, P.L. (2012) High energy resolution five-crystal spectrometer for high quality fluorescence and absorption measurements on an x-ray absorption spectroscopy beamline. Review of Scientific Instruments, 83, 063104.

Mei, Y, Sherman D.M., Liu W., and Brugger J. (2013) Complexation of gold in S_3^--rich hydrothermal fluids: Evidence from ab-initio molecular dynamics simulations. Chemical Geology, 347, 34–42.

Mei, Y., Liu, W.H., Sherman, D.M., and Brugger, J. (2014) Metal complexation and ion hydration in low density hydrothermal fluids: ab initio molecular dynamics simulation of Cu(I) and Au(I) in chloride solutions (25–1000 °C, 1–5000 bar). Geochimica et Cosmochimica Acta, 131, 196−212.

Merkulova, M., Mathon, O., Glatzel, P., Rovezzi, M., Batanova, V., Marion, P., Boiron, M-C., and Manceau, A. (2019) Revealing the chemical form of 'invisible' gold in natural arsenian pyrite and arsenopyrite with high energy-resolution x-ray absorption spectroscopy. ACS Earth Space Chemistry, 3, 1905–1914.

Perdew, J.P., Burke, K., and Ernzerhof, M. (1996a) Generalized gradient approximation made simple. Physical Review Letters, 77, 3865.

Perdew, J.P., Ernzerhof, M., and Burke, K. (1996b) Rationale for mixing exact exchange with density functional approximations. Journal of Chemical Physics, 105, 9982–9985.

Pokrovski, G.S., and Dubrovinsky, L.S. (2011) The S_3^- ion is stable in geological fluids at elevated temperatures and pressures. Science, 331, 1052–1054.

Pokrovski, G.S., and Dubessy, J. (2015) Stability and abundance of the trisulfur radical ion S_3^- in hydrothermal fluids. Earth and Planetary Science Letters, 411, 298–309.

Pokrovski, G.S., Zakirov, I.V., Roux, J., Testemale, D., Hazemann, J.-L., Bychkov, A.Y., and Golikova, G.V. (2002) Experimental study of arsenic speciation in vapor phase to 500°C: Implications for As transport and fractionation in low-density crustal fluids and volcanic gases. Geochimica et Cosmochimica Acta, 66, 3453–3480.

Pokrovski G.S., Roux J., Hazemann J-L., and Testemale D. (2005) An X-ray absorption spectroscopy study of argutite solubility and germanium aqueous speciation in hydrothermal fluids to 500°C and 400 bar. Chemical Geology, 217, 127–145.

Pokrovski G.S., Borisova A.Y., Roux J., Hazemann J.-L., Petdang A., Tella M., and Testemale D. (2006) Antimony speciation in saline hydrothermal fluids: A combined X-ray absorption fine structure and solubility study. Geochimica et Cosmochimica Acta, 70, 4196–4214.

Pokrovski, G.S., Tagirov, B.R., Schott, J., Hazemann, J-L., and Proux, O. (2009a) A new view on gold speciation in sulfur-bearing hydrothermal fluids from in-situ X-ray absorption spectroscopy and quantum-chemical modeling. Geochimica et Cosmochimica Acta, 73, 5406–5427.

Pokrovski, G.S., Tagirov, B.R., Schott, J., Bazarkina, E.F., Hazemann, J.-L., and Proux, O. (2009b) An in situ X-ray absorption spectroscopy study of gold-chloride complexing in hydrothermal fluids. Chemical Geology, 259, 17–29.

Pokrovski, G.S., Akinfiev, N.N., Borisova, A.Y., Zotov, A.V., and Kouzmanov, K. (2014) Gold speciation and transport in geological fluids: insights from experiments and physical-chemical modelling. Geological Society of London Special Publication, 402, 9–70.

Pokrovski, G.S., Kokh, M.A., Guillaume, D., Borisova, A.Y., Gisquet, P., Hazemann, J.-L., Lahera, E., Del Net, W., Proux, O., Testemale, D., Haigis, V., Jonchière, R., Seitsonen, A.P., Ferlat, G., Vuilleumier, R., Saitta, A.M., Boiron, M.-C., and Dubessy, J. (2015) Sulfur radical species form gold deposits on Earth. Proceedings of the National Academy of Sciences of the USA, 112, 13484–13489.

Pokrovski, G.S., Kokh, M.A., Proux, O., Hazemann, J.-L., Bazarkina, E.F., Testemale D., Escoda, C., Boiron, M.-C., Blanchard, M., Ajgouy, T., Gouy, S., de Parseval, P., and Thibaut, M. (2019) The nature and partitioning of invisible gold in the pyrite-fluid system. Ore Geology Reviews, 109, 545–563.

Pokrovski, G.S., Escoda, C., Blanchard, M., Testemale, D., Hazemann, J-L., Gouy, S., Kokh, M.A., Boiron, M-C., de Parseval, F., Aigouy, T., Menjot, L., de Parseval, P., Proux, O., Rovezzi, M., Béziat, D., Salvi, S., Kouzmanov, K., Bartsch, T., Pöttgen, R., and Doert, T. (2021) An arsenic-driven pump for invisible gold in hydrothermal systems. Geochemical Perspectives Letters 17, 39–44.

Proux, O., Lahera, E., Del Net, W., Kieffer, I., Rovezzi, M., Testemale, D., Irar, M., Thomas, S., Aguilar-Tapia, A., Bazarkina, E. F., Prat, A., Tella, M., Auffan, M., Rose, J., and Hazemann, J.-L. (2017) High Energy Resolution Fluorescence Detected X-ray Absorption Spectroscopy: a new powerful structural tool in environmental biogeochemistry sciences. Journal of Environmental Quality, 46, 1146–1157.

Saunders, J.E., Pearson, N.J., O'Reilly, S.Y., and Griffin, W.L. (2018) Gold in the mantle: A global assessment of abundance and redistribution processes. Lithos, 322, 376–391.

Schmidt, C., and Seward, T.M. (2017) Raman spectroscopic quantification of sulfur species in aqueous fluids: Ratios of relative molar scattering factors of Raman bands of H_2S, HS^-, SO_2, HSO_4^-, SO_4^{2-}, $S_2O_3^{2-}$, S_3^- and H_2O at ambient conditions and information on changes with pressure and temperature. Chemical Geology, 467, 64–75.

Seward, T.M. (1989) The hydrothermal chemistry of gold and its implications for ore formation: boiling and conductive cooling as examples. Economic Geology Monograph, 6, 398–404.

Seward, T.M. (1973) Thio complexes of gold and the transport of gold in hydrothermal ore solutions. Geochimica et Cosmochimica Acta, 37, 379–399.

Spezia, R., Bresson, C., Auwer, C.D., Gaigeot, M.-P. (2008) Solvation of Co(III)-cysteinato complexes in water: A DFT-based molecular dynamics study. Journal of Physical Chemistry, B112, 6490–6499.

Spezia, R., Beuchat, C., Vuilleumier, R., D'Angelo, P., Gagliardi, L. (2012) Unravelling the hydration structure of ThX_4 ($X = Br$, Cl) water solutions by molecular dynamics simulations and X-Ray absorption spectroscopy. Journal of Physical Chemistry B116, 6465–6475.

Tagirov, B.R., Trigub, A.L., Filimonova, O.N., Kvashnina, K.O., Nickolsky, M.S., Lafuerza, S., and Chareev, D.A. (2019) Gold transport in hydrothermal chloride-bearing fluids: insights from in situ X-ray absorption spectroscopy and ab initio molecular dynamics. ACS Earth and Space Chemistry, 3, 240–261.

Testemale, D., Hazemann, J.-L., Pokrovski, G.S., Roux, J., Joly, Y., Argoud, R., and Geaymond, O., 2004. Structural and electronic evolution of the $As(OH)_3$ molecule in high-temperature aqueous solutions: an x-ray absorption investigation. Journal of Chemical Physics, 121, 8973–8982.

Testemale, D., Argoud, R., Geaymond, O., Hazemann, J-L. (2005) High pressure/high temperature cell for x-ray absorption and scattering techniques. Review of Scientific Instruments, 76, 043905–043909.

Testemale, D., Pokrovski, G.S., Hazemann, J.-L. (2011) Speciation of As^{III} and As^{V} in hydrothermal fluids by in-situ X-ray absorption spectroscopy. European Journal of Mineralogy, 23, 379–390.

Trigub, A.L., Tagirov, B.R., Kvashnina, K.O., Lafuerza, S., Filimonova, O.N., and Nickolsky, M.S. (2017a) Experimental determination of gold speciation in sulfide-rich hydrothermal fluids under a wide range of redox conditions. Chemical Geology, 471, 52–64.

Trigub, A.L., Tagirov, B.R., Kvashnina, K.O., Chareev, D.A., Nickolsky, M.S., Shiryaev, A.A., Baranova, N.N., Kovalchuk, E.V., and Mokhov, A.V. (2017b) X-ray spectroscopy study of the chemical state of “invisible” Au in synthetic minerals in the Fe-As-S system. American Mineralogist, 102, 1057–1065.

Zajacz Z., Seo J.H., Candela P.A., Piccoli P.M., and Heinrich, C.A. (2010) Alkali metals control the release of gold from volatile-rich magmas. Earth and Planetary Science Letters, 297, 50–56.

Table 1. Summary of the HR-XAS experiments at 350°C and 600 bar conducted in this study.

Run number, starting solution composition (*m*, mol/kg fluid)	**$pH_{T,P}$**	**$\log f_{O_2}$ (vs HM)**	**$\log_{10} m_{Au}$[(a)]**	**Dominant Au species[(b)]**
Exp 1: 0.46m $K_2S_2O_3$ + 0.20m HCl	4.3	+1.1	–2.40	$Au(HS)S_3^-$
Exp 2: 0.51m $K_2S_2O_3$ + 0.29m KOH	7.1	–1.5	–2.14	$Au(HS)_2^-$
Estimated standard error (2 s.d.)	±0.2	±0.2	±0.30	-

Notes: (a) Measured total dissolved Au concentration in solution saturated with metallic gold, derived from the absorption edge height of XAS spectra in transmission and fluorescence modes (see Supplemental Material).

(b) Predicted using thermodynamic modeling (see Fig. 1 for detailed S and Au speciation in the fluid).

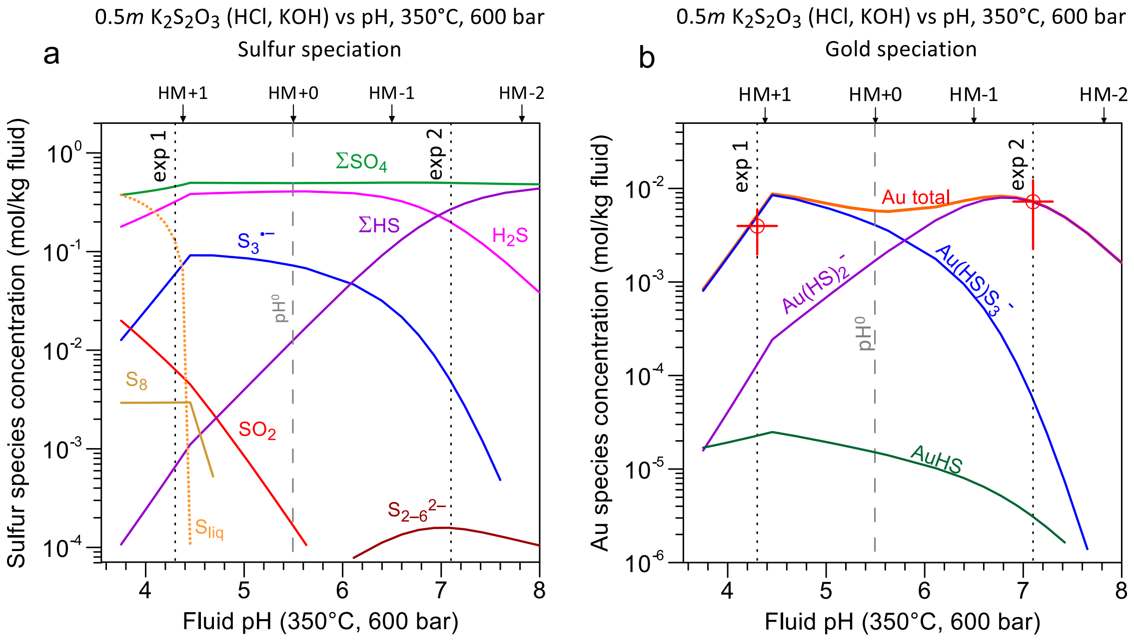

Figure 1. Sulfur (**a**) and gold (**b**) speciation in a 0.5*m* $K_2S_2O_3$ aqueous solution of this study predicted as a function of fluid pH (controlled by addition of KOH or HCl) at 350°C and 600 bar, using the recent thermodynamic data sources (Pokrovski et al. 2015; Kokh et al. 2020; references therein). Vertical dashed line indicates the pH of the neutrality point of water at the given *T* and *P*; vertical dotted lines show the compositions of the two experiments of this study (Table 1). The oxygen fugacity is indicated relative to the hematite-magnetite buffer (HM, in $\log_{10}f_{O2}$ units). ΣSO_4 and ΣHS denote the sum of concentrations of sulfate-type (SO_4^{2-}, KSO_4^-, HSO_4^-, $KHSO_4^0$) and sulfide-type (HS^- and KHS^0) species, respectively. The break in the species curve pattern at pH ~4.4 reflects the onset of molten sulfur (S_{liq}) formation at more acidic pH. Red circles in (**b**) show the average Au solubility measured in the experiments of this study (error bars = standard deviation estimated at 95% probability level; see the Results section).

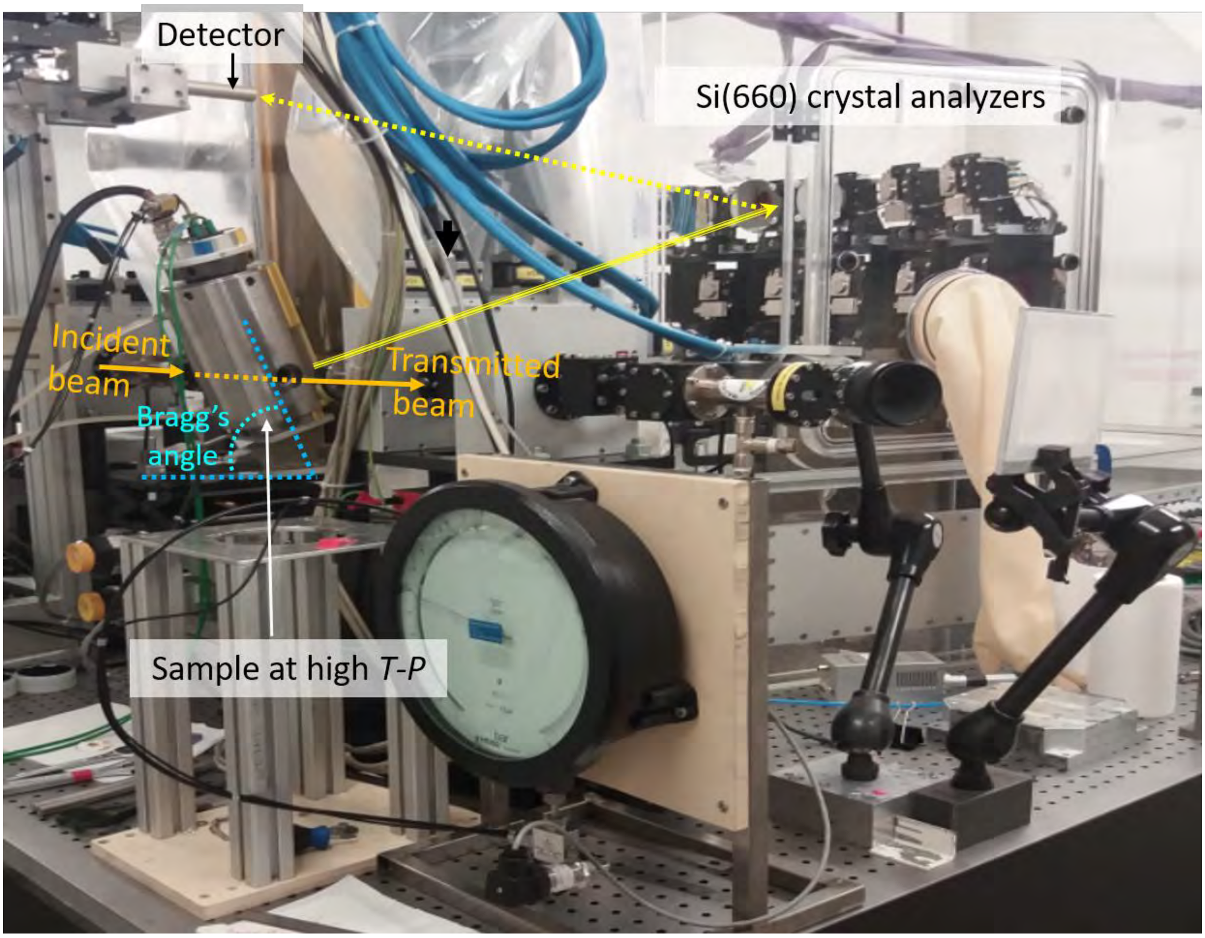

Figure 2. The experimental high-resolution spectroscopic setup at FAME-UHD beamline used in this study. The autoclave is tilted by ~10° from the vertical position to match the required Bragg angle of the crystal analyzers to selectively probe the Au Lα_1 fluorescence line.

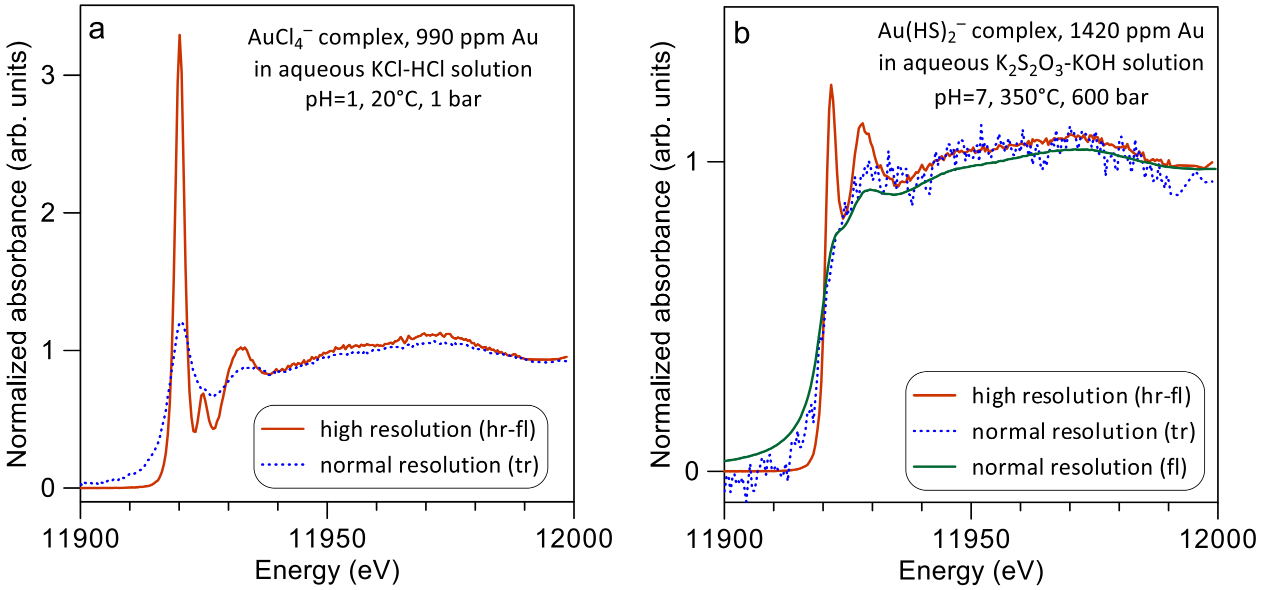

Figure 3. Comparison of Au L_3-edge XANES spectra of aqueous (**a**) auric chloride (calibration solution) and (**b**) aurous sulfide (experiment 2) solutions at the indicated *T*-*P* and composition, recorded in nominal (normal) resolution transmission (tr) and high resolution HERFD (hr-fl) modes. Also shown for comparison is a normal resolution fluorescence spectrum (fl) from a previous experiment at similar *T*, pH and S speciation (exp #3 in Pokrovski et al. 2009a). Note the spectacular improvement in the spectral quality and information in HERFD mode, with each spectral feature neatly emphasized, whereas the normal-resolution spectra are poorly resolved and/or much noisier especially at elevated temperatures (e.g., tr mode in panel b).

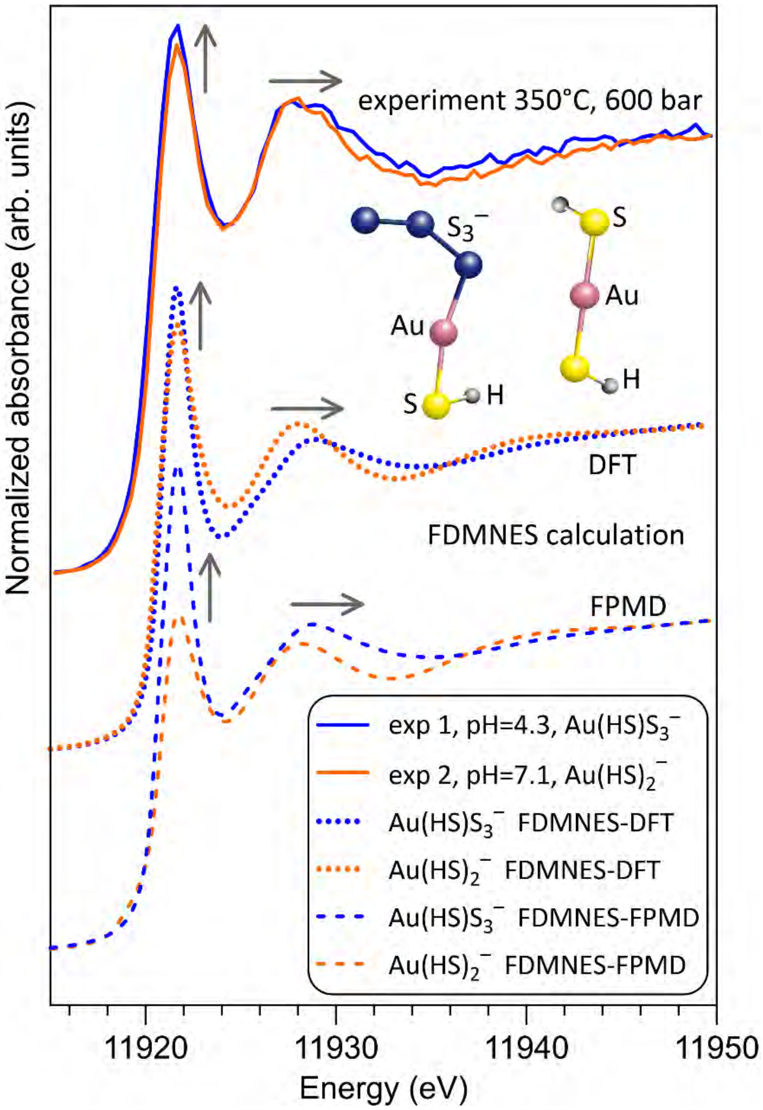

Figure 4. Comparison between measured and calculated Au L_3-edge HR-XANES spectra of aqueous Au species. Measured spectra (solid curves) are from the two experiments of this study at 350°C and 600 bar in acidic (exp 1) and slightly alkaline (exp 2) sulfidic solutions, in which $Au(HS)S_3^-$ and $Au(HS)_2^-$ are predicted to be the major species, respectively (see Fig. 1b). Simulated XANES spectra are obtained by FDMNES calculations using the species structures from DFT geometry optimizations (dotted curves) and shown in ball-and-stick style (Au = pink, S = yellow, S_3 = blue, H = gray), and using the FPMD extracted representative clusters of configurations averaged according to their respective weights (see Supplementary Material). Gray arrows indicate differences in the experimental spectra, showing a slightly higher white-line amplitude and higher-energy broadening of the first post-edge resonance in the acidic solution. The same differences are apparent between the calculated spectra, supporting the change in Au speciation from $Au(HS)S_3^-$ in acidic to $Au(HS)_2^-$ in alkaline solution, which can only be directly revealed by the high-resolution spectroscopic approach.

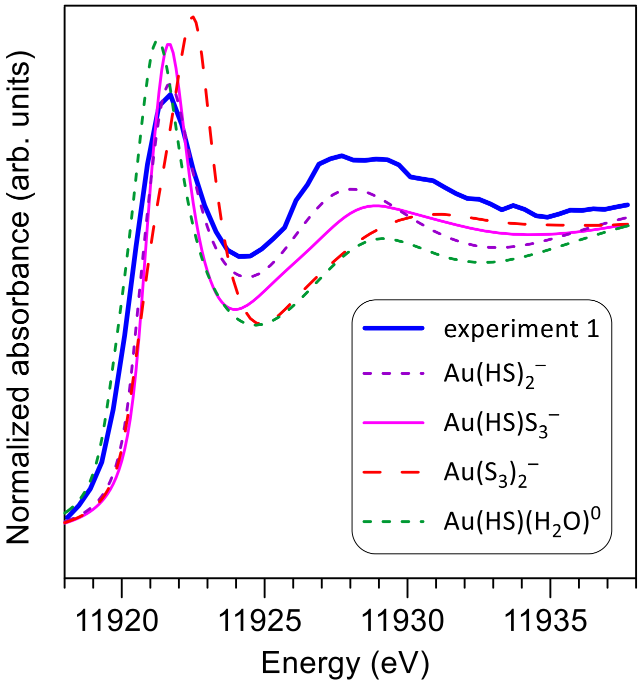

Figure 5. Comparison of the Au L$_3$-edge XANES spectrum measured in the hydrothermal fluid of experiment 1 with FDMNES-simulated spectra of different Au-complexes whose structures are generated by DFT geometry optimizations using the B3LYP functional. The best match of the experimental spectrum is achieved with the Au(HS)S$_3^-$ species, in agreement with thermodynamic calculations of Au speciation and solubility for this experiment (Fig. 1b).